# Lab-Scale Reactor Tests on Fe-Doped $CaMnO_3$ for Thermochemical Heat Storage Application

**Emanuela Mastronardo[1,2], Mario Sánchez[3], José González-Aguilar[3], Sossina M. Haile[4] and Juan M. Coronado[1]**

[1] Engineering Department, University of Messina, Messina (Italy).
[2] Instituto de Catálisis y Petroleoquímica, CSIC, Madrid (Spain).
[3] High-Temperature Processes Unit, IMDEA Energy Institute, Madrid (Spain).
[4] Materials Science and Engineering, Northwestern University, Evanston, IL (United States).

**Abstract**

In order to improve the dispatchability of next-generation concentrated solar power (CSP) plants, $Ca(Fe_{0.1}M_{0.9})O_3$ has been proposed as high temperature (>800 °C) thermochemical energy storage (TES) materials. Only recently, the thermodynamics of $Ca(Fe_{0.1}M_{0.9})O_3$ oxide has been measured through Van't Hoff approach via thermogravimetric (TG) analysis, thus allowing access to the oxygen non-stoichiometry profiles ($\delta(T, pO_2)$) under different temperature and oxygen partial pressure $pO_2$. The material TES performance is here investigated through laboratory scale reactor tests carried out under conditions considered representative of future CSP plants. Remarkably, the material exhibits the same $\delta(T, pO_2)$ profile as the one computed from the thermodynamics at a significantly larger scale (~40g). According to the obtained results, $Ca(Fe_{0.1}M_{0.9})O_3$ oxide appears ideally suited for thermal energy storage applications with a large total (thermochemical and sensible) heat storage capacity (~916 $kJ/kg_{ABO3}$) and good scalability.

*Keywords: thermal energy storage, reactor tests, perovskite, calcium manganite, iron doping*.

## 1. Introduction

Widespread adoption of concentrating solar power (CSP) plants depends considerably on (i) how efficiently solar energy is transformed in electricity collected by means of thermodynamic cycles and (ii) the ability of the plant to store energy and supply power on demand during off-sun periods. The heat-to-electricity conversion efficiency can be enhanced through advanced thermodynamic based on Brayton (*i.e.* $sCO_2$) or combined cycles (*i.e.* air) (Weinstein et al. (2015)), thus requiring high operating temperatures (≥800°C up to 1200 °C). The latter can be put into effect with Thermal Energy Storage (TES) systems. The benefit of high operating temperatures makes a compelling case for designing high-temperature (≥800°C) heat storage systems. TES technologies can be categorized into sensible (latent) heat storage and thermochemical heat storage (TCS). In TCS systems, heat is converted into chemical energy by promoting an endothermic reaction whereby reaction products are stored for a later re-use in the reverse reaction. Different reaction pairs are used to store heat depending on the heat storage target temperature (André et al. (2016)). Additionally, the selection of a proper system is determined by the overall thermodynamic performance and by chemical engineering criteria (kinetics, design factors, etc.), which determine practicability and cost of operation.

Recently, it has been demonstrated that perovskites ($ABO_3$) are promising candidates for high-temperature ThermoChemical heat storage (TCS) applications. A perovskite-based TES system is based on the following reaction:

$$ABO_{3-\delta_i}(s) \rightleftharpoons ABO_{3-\delta_f}(s) + \frac{\delta_f-\delta_i}{2}O_2(g) \qquad \text{(eq. 1)}$$

where, $\delta_0$ is the initial oxygen nonstoichiometry, and $\delta_f$ is the nonstoichiometry at the completion of the reduction/oxidation process. The $ABO_3$ oxide reduction/oxidation reaction can occur through continuous oxygen release/uptake over a broad temperature window with the formation/destruction of oxygen vacancies within the material's structure.

Babiniec et al. studied $La_xSr_{1-x}Co_yM_{1-y}O_{3-\delta}$ (M=Mn, Fe) compositions, with $0.1 \leq x \leq 0.9$ and $0.1 \leq y \leq 0.9$ (Babiniec et al. (2015)). They showed interesting heat storage capacity and placed this class of materials among the candidates for high-temperature TES systems. The potential of $SrBO_{3-\delta}$ and $BaBO_{3-\delta}$ (B=Mn, Fe, Co) oxides as TES materials


doi:10.18086/swc.2021.33.05 Available at http://proceedings.ises.org

has been investigated by Zhang and co-workers (Zhang et al. (2016)). The analogous material, $CaMnO_3$, has attracted high interest because, being based on earth-abundant elements, it is cost-effective (Babiniec et al. (2015), Imponenti et al (2017), Mastronardo et al. (2020), Torres et al. (2019)). B-site doping with Fe (Mastronardo et al (2020), Mastronardo et al. (2019)), Al (Babiniec et al. (2015)), Ti (Babiniec et al. (2015)), Co (Jin et al. (2021)) and Cr (Lucio et al. (2019)) enhanced the heat storage capacity relative to that of undoped $CaMnO_3$. Of these materials, $Ca(Fe_{0.1}Mn_{0.9})O_3$ has been studied by thermogravimetric analysis (TGA) and its thermodynamics determined through the Van't Hoff approach (Mastronardo et al. (2020)). In comparison to other dopants, Fe enables operation at higher temperature and more moderate $pO_2$ for a comparable level of heat storage (Mastronardo et al (2020), Mastronardo et al. (2019)). Additionally, its stability was assessed by long-term (~80h) cycling between reduction and subsequent reoxidation to simulate the operating conditions. These attractive features warranted further investigation. Indeed, large scale reactor tests are fundamental to bring the perovskites TCS systems to a level closer to the market (Pan et al. (2017)). In this regard, several research activities are focused on design and development of TES pilot plant tests (Jackson et al. (2019), Schrader et al. (2020)).

We carry out here an evaluation of $Ca(Fe_{0.1}Mn_{0.9})O_3$ heat storage performance through lab-scale reactor tests at significantly larger scale than previously reported and under conditions considered realistic according to the design features of future power plants.

## 2. Materials and Methods

### 2.1 Material preparation and characterization

About 40 g of $Ca(Fe_{0.1}Mn_{0.9})O_3$ oxide, hereafter CMF91, was prepared according to a modified Pechini method reported in the literature (Mastronardo et al. (2020)). The CMF91 powder was mixed and ground with 5% wt. of carboxymethylcellulose (CMC), and then mixed with a specific amount of water to obtain a plastic paste. The paste was extruded through a cylindrical die of 0.3mm Ø and cut into pieces of ~1 cm length. The pellets were sintered at 1100 °C (heating/cooling rate 3°C/min) for 8h under static air and the CMC fully decomposed (verified by X-Ray Diffraction – XRD – analysis). The resulting porous CMF91 pellets were characterized by Mercury Intrusion Porosimetry (MIP) analysis and Scanning Electron Microscopy (SEM).

### 2.2 Lab-scale reactor apparatus and tests

The lab-scale reactor for testing heat storage suitability (Figure 1) consists of a customized high-temperature furnace, an alumina reactor tube (length 1.2m, $Ø_{external}$ 30mm, $Ø_{internal}$ 24mm), a cooling system, and a Micro Gas Chromatographer (mGC) that samples the $O_2$ concentration. The reactor tube is filled from the bottom to a selected height with chunks of alumina foam so that the material bed is allocated in the furnace's middle isothermal zone. The supplied gas flows from the top to the bottom of the tubular reactor and is analyzed through the mGC. In a typical experiment, the material is heated up to a selected reduction temperature ($T_r$), and, after a hold time of 30 minutes, it is cooled down to the oxidation temperature ($T_o$). Several tests were carried out varying $pO_2$, $T_r$, and gas flow rate. The $O_2$ evolution while heating and cooling was measured, and a comparison between $\delta(T)$ profiles obtained by lab-scale reactor test (~40 g) and thermogravimetric analysis (~500 mg) was carried out to verify the material's thermochemical performance at a significantly larger mass scale.

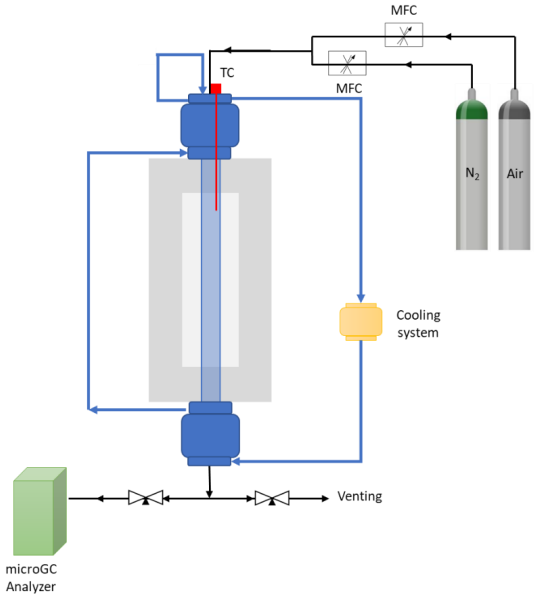


**Fig. 1: Scheme of the lab-scale reactor apparatus.**

In order to calculate the material oxygen evolution profile obtained from the reactor tests, the instant oxygen concentration recorded by mGC analyzer is subtracted from the average supplied $O_2$ flow concentration:

$$\Delta O_{2_i}(\%/\text{min}) = O_{2_{ist}} - O_{2_{avg}} \qquad \text{(eq. 2)}$$

The oxygen evolution is converted in mol/min (equ. 3), and the cumulative value is obtained by the integration over time (equ. 4):

$$\Delta O_{2_i}\left(\frac{\text{mol}}{\text{min}}\right) = \frac{\Delta O_{2_i}(\%/\text{min})\cdot \dot{V}(\text{nL}/\text{min})}{22.4136(\text{mol}^{-1})} \qquad \text{(eq. 3)}$$

$$\Delta mO_{2_i}(g) = M_{O_2}\cdot \int_{t_0}^{t_i} \Delta O_2 dt \qquad \text{(eq. 4)}$$

being $\dot{V}$(nL/min) the total flow rate.

The equilibrium oxygen nonstoichiometry is calculated according to equation 5:

$$3\text{-}\delta_i = 3\text{-}\delta_0 + \left(\frac{\Delta mO_{2_i}}{M_O \cdot n_{ABO3}}\right) \qquad \text{(eq. 5)}$$

where ($\delta_0$) is the material initial oxygen nonstoichiometry at the specific $T_o$ and $pO_2$ used – extracted from the available thermodynamics data (Mastronardo et al. (2020)) –, $M_O$ (g/mol) is the monoatomic oxygen mass, and $n_{ABO3}$ (mol) are the moles of material.

## 3. Results and Discussion

Hg porosimetry results are shown in Fig. 2a. The incremental Hg intrusion plot as a function of the pore diameter shows three peaks, all in the macropore range, centered around 2, 4 and 10 μm, respectively. The Hg intrusion in the low-pressure region (ca. 0.1–10 μm) is due to the interparticle voids and cracks, which can also be observed on the surface of pellets by SEM analysis (Fig. 2b). The as prepared pellets have a total pore volume and area of 0.36 ml/g and 0.54 $m^2$/g, respectively, a bulk density of 3.58 g/ml, and a porosity of 56% thus guaranteeing easy gas access to the entirety of the material that is an essential feature for eventual technological deployment.

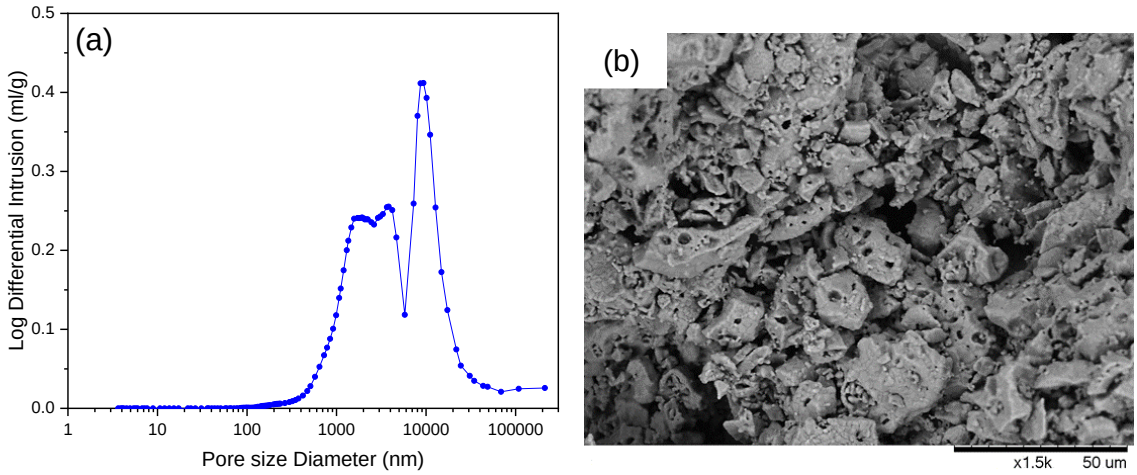


**Fig. 2: (a) Incremental intrusion plotted against pore diameter and (b) SEM micrograph of CMF91 pellets prepared with the addition of 5% of CMC.**

Fig. 3 shows the comparison between the heating/cooling δ(T) profiles obtained by lab-scale reactor test and thermogravimetric (TG) analysis previously performed (Mastronardo et al. (2020)). Heating and cooling profiles overlap, indicating complete reversibility. Also, remarkably, the profiles obtained by lab-scale reactor test matches fairly well with the TG profile, indicating results reproducibility using a mass (~40g) two orders of magnitude larger than the one used in TG (~0.5g). Thus, not only does the material releases oxygen up to its thermodynamic limit (determined by the operating conditions), but also it remains equilibrated in the lab-scale reactor environment for the gas flow and heating rates employed..

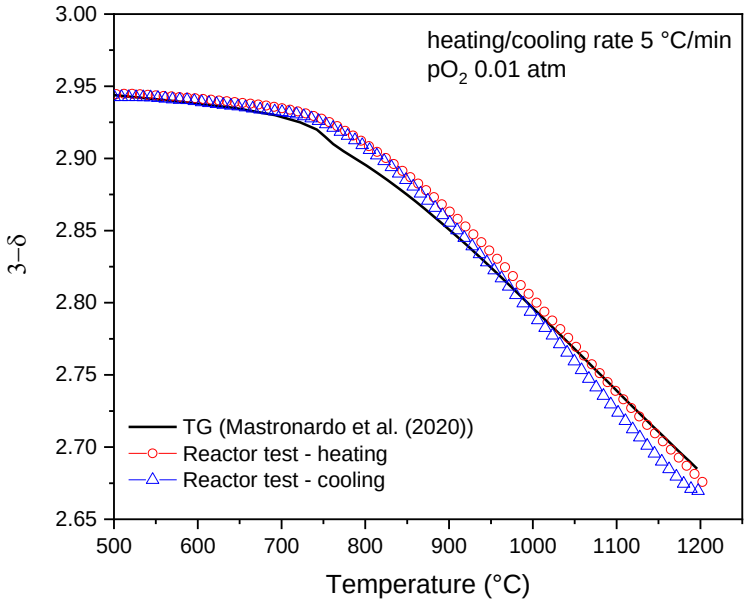


**Fig. 3: δ(T) profiles of CMF91 material determined by mGC and compared to TG analysis profile (Mastronardo et al. (2020)).**

The material chemical heat storage capacity is calculated as:

$$Q_C\left(\frac{kJ}{kg_{ABO3}}\right)=\frac{1}{M_{ABO3}}\int_{\delta_i}^{\delta_f}\Delta_{red}h\left(\frac{kJ}{mol_O}\right)d\delta \qquad \text{(eq. 6)}$$

where $M_{ABO3}$ is the molar mass of the oxide, $\Delta_{red}h$ is the enthalpy of reduction associated with reaction (1) and has been evaluated in a previous thermodynamic study (Mastronardo et al. (2020)), $\delta_i$ is the initial oxygen non-stoichiometry (at T = $T_O$) and $\delta_f$ is the nonstoichiometry at the final condition of interest, here taken to be T=$T_R$.

Using the known thermodynamic properties of CMF91, chemical heat storage capacity of ~356 kJ/$kg_{ABO3}$ is estimated. Taking into account the sensible heat, the total heat storage capacity of the material ($Q_{tot}$) is:

$$Q_{tot}\left(\frac{kJ}{kg_{ABO3}}\right)=Q_C+\int_{T_O}^{T_R} C_P\,dT \qquad \text{(eq. 7)}$$

where $C_p$ is the material's heat capacity. CMF91 total heat storage capacity in the temperature range 500-1200 °C under a $pO_2$ of 0.01 atm is ~916 kJ/$kg_{ABO3}$.

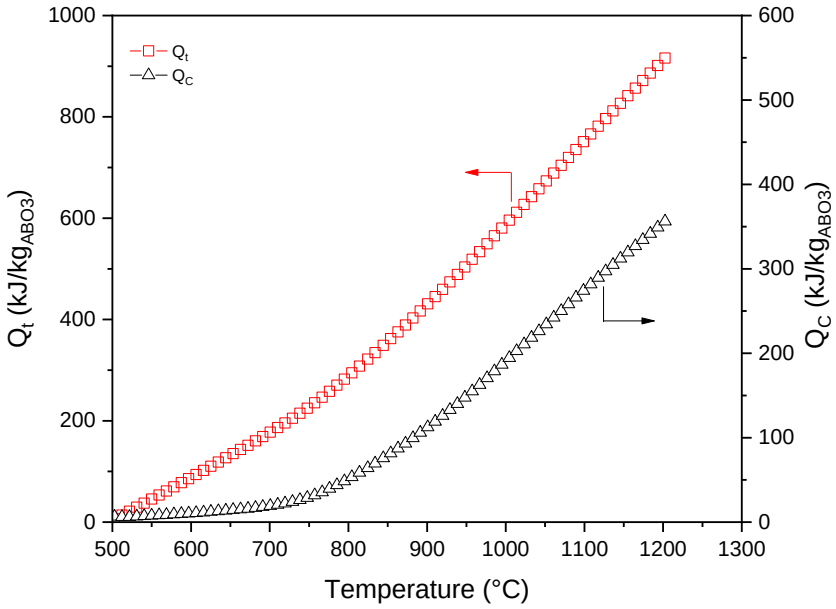


**Fig. 4: Total ($Q_t$) and chemical ($Q_c$) heat storage capacity of the material as a function of temperature.**

## 4. Conclusions

The heat storage capacity of CMF91 pellets has been evaluated through a lab-scale thermochemical heat storage reactor. Remarkably, it was evidenced that the material at a significantly larger scale (two orders of magnitude larger) was able to exhibit the same performance than the one measured through thermogravimetric analysis. According to these results, CMF91 appears ideally suited for thermochemical heat storage applications with a high total heat storage capacity (~916 kJ/$kg_{ABO3}$) and good scalability.

## 5. Acknowledgments

This project has received funding from the European Union's Horizon 2020 research and innovation programme under the Marie Sklodowska-Curie grant agreement N° 74616. Support of the ACES2030 from "Comunidad de Madrid" and European Structural Funds to (P2018/EMT-4319), and of the US Department of Energy, Office of Energy Efficiency and Renewable Energy, Award DE-EE0008089.0000 are also fully acknowledged.

## References

André, L., Abanades, S., Flamant, G., 2016. Screening of thermochemical systems based on solid-gas reversible reactions for high temperature solar thermal energy storage, Renew. Sustain. Energy Rev. 64, 703–715.

Babiniec, S.M., Coker, E.N., Miller JE, Ambrosini A., 2015. Investigation of $La_xSr_{1-x}Co_yM_{1-y}O_{3-\delta}$ (M=Mn, Fe) perovskite materials as thermochemical energy storage media. So.l Energy118, 451–459.

Babiniec, S.M., Coker, E.N., Miller JE, Ambrosini A., 2015. Doped calcium manganites for advanced high-temperature thermochemical energy storage. Int. J. Energy Res 40, 6–10.

Imponenti, L., Albrecht, K.J., Wands, J.W., Sanders, M.D., Jackson, G.S., 2017. Thermochemical energy storage in strontium-doped calcium manganites for concentrating solar power applications. Sol. Energy 151 1-13.

Jackson, G.S., Imponenti, L., Albrecht, K.J., Miller, D.C., Braun, R.J., 2019. Inert and Reactive Oxide Particles for High-Temperature Thermal Energy Capture and Storage for Concentrating Solar Power. J. Sol. Energy Eng. Trans. ASME. 141.

Jin, F., Xu, C., Yu, H., Xia, X., Ye, F., Li, X., et al., 2021. $CaCo_{0.05}Mn_{0.95}O_{3-\delta}$: A Promising Perovskite Solid Solution for Solar Thermochemical Energy Storage. ACS Appl. Mater. Interfaces 13, 3856–3866.

Lucio, B., Romero, M., González-Aguilar, J., 2019. Analysis of solid-state reaction in the performance of doped calcium manganites for thermal storage. Solid State Ion. 338, 47–57.

Mastronardo, E., Qian, X., Coronado, J.M., Haile, S.M., 2020. The favourable thermodynamic properties of Fe-doped $CaMnO_3$ for thermochemical heat storage. J. Mater. Chem. A 8, 8503-8517.

Mastronardo, E., Qian, X., Coronado, J.M., Haile, S., 2019. Fe-doped $CaMnO_3$ for thermochemical heat storage application. AIP Conf Proc 2126, 210005-210008.

Pan, Z.H., Zhao, C.Y., 2017. Gas–solid thermochemical heat storage reactors for high-temperature applications, Energy 130, 155–173.

Schrader, A.J., Schieber, G.L., Ambrosini, A., Loutzenhiser, P.G., 2020. Experimental demonstration of a 5 kWth granular-flow reactor for solar thermochemical energy storage with aluminum-doped calcium manganite particles, Appl. Therm. Eng. 173, 115257.

Torres, A., Luque, F.J., Tortajada, J., Arroyo-de Dompablo, M.E., 2019. DFT investigation of Ca mobility in reduced-perovskite and oxidized-marokite oxides. Energy Stor. Mater. 21, 354–360.

Weinstein, L.A., Loomis, J., Bhatia, B., Bierman, D.M., Wang, E.N., Chen, G., 2015. Concentrating Solar Power. Chem. Rev. 115, 12797-12838.

Zhang, Z., Andre, L., Abanades, S., 2016. Experimental assessment of oxygen exchange capacity and thermochemical redox cycle behavior of Ba and Sr series perovskites for solar energy storage. Sol Energy 134, 494–502.